Chapter-2

Experimental and Computational Methods

2.1 Introduction

This chapter provides detailed descriptions of the experimental and computational procedures used in the research work presented in this thesis. It includes the specifications of the instruments utilized for characterizing the prepared samples and the experimental setups and methods applied in various applications. Additionally, the experiments conducted for simultaneous adsorption and photo-Fenton degradation of organic pollutants are discussed comprehensively. Furthermore, the computational methodologies adopted in this thesis are presented later in the chapter.

2.2 The material characterization with instrumentation details

2.2.1 Powder X-Ray Diffraction (XRD)

The XRD pattern of the synthesized samples was obtained using the Rigaku Mini Flex 600 desktop X-ray diffraction equipment. This is a non-destructive process. It is generally used to determine crystalline phases, crystallite size, interplanar distance, and lattice strains in the material. The main parts of this equipment are an X-ray generating source, optics, a goniometer, and a detector. In this thesis, Cu-Kα radiation with a wavelength of 1.54059 Å was employed for all XRD measurements. Diffraction data were typically acquired at a scan rate of 5° per minute for 2θ angles, ranging from 5 to 90, with a 0.01 step size. The XRD patterns' peaks were matched with JCPDS files to identify the phase of the prepared samples. Bragg's equation[122] was used to calculate the interplanar d-spacing (Equation 2.1).

$$n\lambda = 2d\ sin\ \theta \quad \ldots\ldots\ldots\ldots\ldots\ldots\ldots\ldots\ldots\ldots \quad \ldots\ldots(2.1)$$

In equation 2.1, n is the order of reflection, λ is the incident radiation wavelength, d denotes the inter-planar spacing, and θ (Bragg angle) represents the angle between the incident ray and the crystallographic plane.

2.2.2 Transmission electron microscope (TEM)

Nanoscale images obtained with a Transmission Electron Microscope (TEM) on a Tecnai G2 20 TWIN instrument (EDAX Inc.) were used to study the morphology and crystal structure of the as-prepared samples. For the TEM measurements, 2 mg of nanoparticles were first dispersed in 2 mL of high-purity ethanol and sonicated for 30 minutes in a water bath. After sonication, 2 μL of the suspension was placed onto a carbon-coated 400-mesh copper/nickel grid (Ted Pella Inc.). The grid was dried in an oven at 60°C for 24 hours before microscopic examination. The resulting images revealed the average particle sizes and morphologies of the samples. The average particle sizes and the d-spacing of the lattice fringes were measured using ImageJ software and TEM micrographs.

2.2.3 Scanning electron microscope (SEM) and Energy dispersive X-ray (EDX)

The morphology and elemental distribution of the as-prepared samples were analyzed using SEM and EDX. For these measurements, a small amount of the powdered sample was evenly spread on carbon tape, and excess material was removed using an air duster. The prepared sample stub was then placed in the SEM chamber for analysis. As the beam of electron interacts with the sample, it produces various signals that reveal detailed information about the surface's topography and composition. A typical SEM setup consists of five key components: (1) an electron source, (2) a column with electromagnetic lenses to control the electron beam, (3) a sample chamber, (4) an electron detector, and (5) a computer for image acquisition and display.

On the other hand, EDX is used to recognize the elements present in a sample and determine their relative concentrations. X-ray generation in EDX involves a two-step process: In first step, the energy transferred to an atomic electron ejects it, creating a vacancy. In second step, this vacancy is filled by an electron from a higher energy shell, releasing energy in the form of a characteristic X-ray, which is then detected and analyzed. The SEM images and EDX data presented in this thesis were obtained using the Nova NanoSEM 450 manufactured by the FEI Company.

2.2.4 X-ray photoelectron spectroscopy (XPS)

The oxidation states and composition of the samples were analyzed by X-ray photoelectron spectroscopy (XPS) using a K-Alpha instrument (the Thermo Fisher Scientific company). The sample for XPS analysis was prepared following a standard procedure. The powdered material was carefully dispersed in ethanol and then drop-cast onto a square glass slide. Then, the glass slide was subsequently dried in a hot air oven to form a thin film of the sample, which was then used for XPS measurements. XPS spectrum measurement involves irradiating a solid surface with X-ray beam and calculating the electron's kinetic energy emitted from the material's surface. The electron's kinetic energy depends on both photon energy ($h\nu$) and its binding energy (or energy required to eject that electron from the surface). As a result, a photoelectron spectrum is created by counting the electrons ejected at various kinetic energies. All spectra were calibrated with the adventitious carbon signal at binding energy 284.8 eV using Casa XPS software.

2.2.5 Vibrating sample magnetometer (VSM)

A vibrating sample magnetometer (VSM) recorded the sample's magnetic properties at room temperature. This instrument operates on the principle of Faraday's Law

of Induction. The sample is placed in a constant magnetic field, causing its magnetization to align if it is magnetic. As the sample moves up and down, its magnetic dipole moment generates a magnetic field that varies with time [123]. In a VSM, the alternating magnetic field induces an electric field in the pickup coils due to the motion of the magnetized sample. The resulting current is proportional to the sample's magnetization, allowing for precise measurement of magnetic properties. As a result, the Hysteresis loops of the materials and the magnetization curve were recorded with respect to applied magnetic field.

2.2.6 Brunauer-Emmett-Teller (BET)

The sample's surface area was obtained by Brunauer-Emmett-Teller (BET) analysis using BELLSORP MAX II & BELCAT-II (MicrotracBEL Corp.) instruments. The concept of the BET theory is an extension of the Langmuir theory to multilayer adsorption[124]. The specific surface area is determined using the BET method by analysing the amount of nitrogen desorbed as the sample, initially cooled to liquid nitrogen temperature under a helium-diluted nitrogen flow, is gradually warmed back to room temperature. In the BET plot, the adsorbed amount is shown on the vertical axis and is usually related to the mass of the adsorbent, while the relative pressure represents by the horizontal axis (p/p_0; p = equilibrium pressure and p_0 = saturation vapor pressure). Generally, the nature and types of sorption isotherms deliver information about the specific surface area, pore volume, and pore size distribution.

2.2.7 Fourier-transform infrared spectroscopy (FTIR)

The Fourier-transform infrared spectroscopy (FTIR) analysis was utilized to identify the functional groups in the prepared sample via the Nicolet iS5 (THERMO Electron Scientific Instruments LLC.) instrument. The powder sample was mixed with KBr in an agate mortar and pestle, followed by pelletization for FT-IR analysis. The spectra

were recorded within the spectral range of 4000 to 400 cm^{-1}, with a resolution of 0.09 cm^{-1}. According to the fundamental selection rule in FTIR spectroscopy, a vibrational mode is only considered infrared-active if it causes a change in the molecule dipole moment [125]. An infrared spectrum acts as a fingerprint for a particular sample, displaying absorption peaks that correspond to the bending and stretching frequencies of vibrations due to bonds in the material. Since every material has a unique atomic combination, it produces a distinctive infrared spectrum. As a result, different materials can be easily identified using infrared spectroscopy, making it an effective tool for qualitative analysis.

2.2.8 UV-Diffuse reflectance spectroscopy (UV-DRS)

Solid-state UV-visible measurements in the 200–800 nm range were performed using a Shimadzu Pharmaspec UV-1700 spectrophotometer. The optical bandgap of the synthesized nanostructures was determined from the Tauc plot derived from the solid-state absorption spectrum [126]. The Tauc plots have been generated using the following equation 2.2:

$$(\alpha h\upsilon)^{1/n} = (h\nu - E_g) \quad \text{..... (2.2)}$$

In equation 2.2, α denotes the molar absorption coefficient, E_g signifies the material bandgap, and υ represents the frequency of light. A photocatalyst's optical band gap (Eg) energy is determined by the intercept of the linear component of the plot $(\alpha h\upsilon)^{1/n}$ versus hυ on the abscissa. The exponent n defines the type of optical transition. The n value is equal to ½ for a direct transition and 2 for an indirect transition.

2.2.9 UV-visible spectrophotometer

Adsorption spectra of all supernatant during all experiments were observed by a UV-visible spectrophotometer (Agilent Cary 60). This spectrophotometer has two light sources. A tungsten lamp scans the visible range (325-770 nm), while a deuterium or

hydrogen discharge tube covers the UV region (200-370 nm). Light can be absorbed, transmitted, or reflected when it passes through a sample solution. Light absorption leads to electronic excitations, such as n-π*, π-π*, n-σ*, involving transitions between non-bonding (n), bonding (π), and anti-bonding orbitals (π* or σ*). A chromophore is a molecular group, typically containing a π bond, that is capable of absorbing UV-visible light. Saturated hydrocarbons do not exhibit UV-visible absorbance. Introduction of a chromophore, typically containing a π bond, allows the compound to absorb light in the 185–1000 nm range. This absorption is detected and recorded as an absorbance spectrum by the UV-visible spectrophotometer. Conjugation of the chromophore's double bonds with extended double bonds increases both intensity and wavelength of the absorption band. This is due to the extended delocalization of π electrons, which lowers the energy gap between molecular orbitals. In UV-Vis spectroscopy, absorbance is commonly measured because it has a linear relationship with concentration, as described by the Beer–Lambert law[127]. In Chapters 4 and 5 of this thesis, multicomponent analyses using UV-visible spectra were also performed. All samples used in this thesis were suitably diluted before being placed in a quartz cuvette with a path length of 1 cm for UV-visible measurements.

2.2.10 Electrochemical analyzer/workstation

The electrochemical analysis of the prepared photocatalysts was conducted using a Metrohm Autolab M204 instrument. The data obtained from this analysis were employed in this thesis to generate Mott-Schottky (MS) plots and perform Electrochemical Impedance Spectroscopy (EIS). For these measurements, a carbon electrode was used as the counter electrode, an Ag/AgCl electrode acts as the reference electrode, and fluorine-doped tin oxide (FTO) acts as the working electrode. The photocatalyst powder was drop-

cast onto an FTO substrate to prepare the sample for Mott-Schottky and EIS measurements. The MS plots were analyzed to determine the flat-band potential of the semiconductor photocatalyst. The slope of the MS plots provides information on the type of semiconductor material, indicating whether it is p-type or n-type[128]. A positive slope typically signifies n-type behavior, whereas a negative slope indicates p-type behavior[128]. Meanwhile, the Nyquist plots obtained from the EIS measurements revealed insights into the charge transfer resistance kinetics of the photocatalysts, providing a deeper understanding of their electrochemical behavior.

2.2.11 Zero-point charge analysis

The salt titration method was used to find the point of zero charge pH (pH_{pzc}) value [129]. First, 200 ml of 0.1M of $NaNO_3$ was prepared, and 20 ml of this solution was poured into eight conical flasks. The initial pH of the $NaNO_3$ solutions in these flasks was then adjusted to values ranging from 2 to 12 using 0.1M HNO_3 and 0.1M NaOH solution. Then, 0.005g of adsorbent was mixed into each conical flask. These mixtures were agitated in a shaker for 24 hours. After that, the final pH of each mixture was carefully measured by a pH meter. Then, the ΔpH (final pH - initial pH) was plotted against initial pH values. The initial pH, at which the ΔpH value is zero, will be the pH_{pzc} of the adsorbent.

2.3 Chemicals used in the sample preparation and different experiments

All chemicals used in this thesis were of analytical grade and employed without any additional purification. The experiments were carried out using double-distilled water with a pH of approximately 6.8. Details of the chemicals utilized in the experimental work have been provided in the Chapters 4, 5, 6, and 7, aligning with the respective sample preparation sections.

2.4 Procedure followed for various applications

2.4.1 Procedure followed for adsorption and simultaneous adsorption

The detailed procedure used for the adsorption of organic pollutants has been mentioned in chapters 4 and 5. In these chapters, several batch experiments have been performed for adsorption in individual or binary adsorbate systems by $NiFe_2O_4$/GO nanocomposite and Mo-doped $NiFe_2O_4$ nanoparticles. The optimization experiments were conducted at various adsorbate solution pH and adsorbent doses. Thereafter, by using optimum adsorbent dose and adsorbate solution pH, adsorption kinetics and adsorption isotherm experiments were conducted. In all adsorption experiments, the thermostatic agitator or the shaker (by Narang Scientific Works PVT. LTD.) was operated at 150 rpm and 300K temperature.

The Simultaneous Equation method, or Vierodt's method, (proposed by N. Erk in 1999) was used to calculate the concentrations of CIP and MG in a mixed solution before and after adsorption [130,131]. The CIP and MG do not interact with each other as required for applying the Beer-Lambert law. A brief description of this method has been given below.

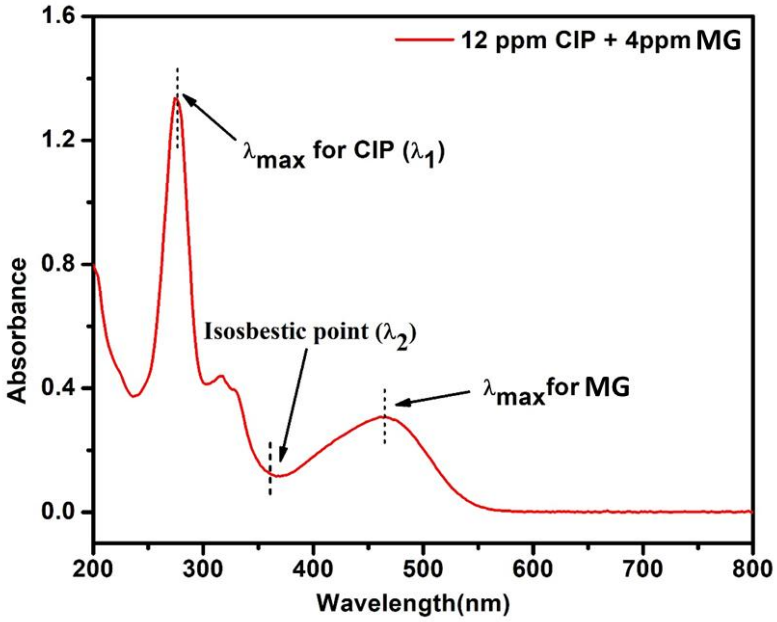

Figure 2.1. A UV-visible spectrum of the binary solution of CIP and MG.

Equations 2.3 and 2.4 give expressions for determining the concentrations of CIP (C_x) and MG (C_y) in their binary solutions.

$$C_x = \frac{(A_2 a_{y1} - A_1 a_{y2})}{(a_{x2} a_{y1} - a_{x1} a_{y2})} \quad \text{.....(2.3)}$$

$$C_y = \frac{(A_1 a_{x2} - A_2 a_{x1})}{(a_{x2} a_{y1} - a_{x1} a_{y2})} \quad \text{.....(2.4)}$$

The first step of finding the parameters in these equations was to select two wavelengths, λ_1 and λ_2, in the binary solution UV-visible absorbance curve. The first wavelength λ_1 was taken at 276.75 nm, while the second wavelength λ_2 was the isosbestic point (359.72 nm) of the binary solution absorbance curve (Figure 2.1). The isosbestic point is the wavelength at which the absorbance of individual CIP and MG have the same value. Next, separate calibration plots of pure aqueous MG and CIP solutions were drawn at λ_1 and λ_2. The absorptivity of CIP at λ_1 and λ_2 is denoted by a_{x1} and a_{x2}. Similarly, the absorptivity of MG at λ_1 and λ_2 is denoted by a_{y1} and a_{y2}. These absorptivity values were calculated from the CIP and MG calibration plots at λ_1 and λ_2 wavelengths. A_1 and A_2 are the absorbance values at λ_1 and λ_2 in the binary (mixed) solution spectrum. The UV-visible spectrum for each binary solution with a particular composition can be analysed by taking the absorbance value A_1 and A_2 at λ_1 and λ_2 wavelengths.

2.4.2 Procedure followed for Fenton and Photo-Fenton processes

The detailed procedure used for Fenton and photo-Fenton degradation of pollutant has been mentioned in Chapter 6 and 7. The Fenton and photo-Fenton catalytic activities of Mo doped $NiFe_2O_4$ nanoparticles and $AgI/NiFe_2O_4$ composite were evaluated for the degradation of the antibiotic - tetracycline. Heterogeneously catalyzed Fenton reactions were carried out in the dark, while visible light irradiation was used for photo-Fenton

reactions. The visible light source was a 14W(Philips) cool white LED bulb fixed in a homemade cubic photocatalytic chamber. The TM-206 solar power meter (pyranometer) model was used to measure the radiation flux density of cool white LED light. The temperature inside the photocatalytic chamber was kept constant at 303 K during the reactions. The turnover frequency (TOF) value and H_2O_2 normalized TOF (HTOF) value of the photocatalysts were calculated to quantitatively evaluate their catalytic efficiency. Equations 2.5 and 2.6 were used to calculate all TOF and HTOF values mentioned in this thesis.

$$TOF = \frac{\left[\frac{Number\ of\ moles\ of\ reactant}{Number\ of\ grams\ of\ catalyst}\right] \times Yield}{time} \qquad (2.5)$$

$$HTOF = \frac{\left[\frac{Number\ of\ moles\ of\ reactant}{Number\ of\ grams\ of\ catalyst}\right] \times Yield}{time \times [moles\ of\ H_2O_2\ per\ litre]} \qquad (2.6)$$

2.5 Computational part

2.5.1 Molecular dynamics simulation

This section provides the main features of classical Molecular Dynamics (MD) simulations. Molecular Dynamics (MD) simulation is a computational technique used to study systems at the atomic level. It provides detailed insights that are inaccessible to obtain through experimental methods. These simulations capture dynamic information about atomic and molecular motions over time, enabling the prediction of thermodynamic properties (such as temperature, pressure, and free energy) and kinetic properties (such as reaction rates and diffusion coefficients)[132]. Classical MD simulations rely on the equations of classical mechanics and are limited to molecular assemblies or interactions without the creation or rupture of chemical bonds [132]. These simulations track the time evolution of interacting atoms by integrating their equations of motion based on Newton's laws [133]. This

allows the trajectories calculation in a multi-dimensional phase space to determine the energy and dynamics of systems with a large number of atoms. In MD simulations, an observable quantity must be stated as a function of the positions and momenta of the particles in the system to be measurable [133].

The first step in the MD simulation is to prepare the initial model system by specifying the initial temperature, the number of molecules, density, simulation run time, and time step magnitude[113]. The criterion for selecting the initial system (the set of positions of molecules constituting the system) configuration is that it should have a finite probability of occurrence under the given temperature and other ensemble conditions. Energy minimization is a crucial preprocessing step before running a molecular dynamics (MD) simulation. This process ensures that the initial structure is physically reasonable and free from large strains or bad contacts, which could lead to numerical instabilities or unrealistic dynamics during the simulation. For that reason, before the simulation run, the model was subjected to minimizing its initial energy using tools like steepest descent or conjugate gradient minimization to remove residual strains or artifacts. When equilibrium is reached after molecular dynamics (MD) simulation, the system has typically settled into a state where its macroscopic properties (e.g., temperature, pressure, and energy) fluctuate around stable averages.

Assigning a force field to the intended MD simulation is a crucial initial step. A force field is a set of empirical energy functions and parameters used to calculate the potential energy as a function of the molecular coordinates [134]. The forces are obtained from a potential energy function's gradient (derivative), defined by a molecular mechanics force field. The Verlet Algorithm efficiently calculates new positions and velocities [134]. The simulation

progresses by iteratively calculating forces, updating positions and velocities, and logging the trajectory for analysis.

This thesis uses periodic boundary conditions with reasonable cut-offs for all simulations. Periodic boundary conditions require that the central system (or simulation box) be surrounded by identical or replica simulation cells. When any atom in the unit cell moves across the boundary, it reappears on the opposite side at the same radial position with respect to the center point. This approach eliminates the edge effects and provides a realistic approximation of bulk material properties. The simulations are conducted for a long enough period to produce reliable ensemble averages. Therefore, systems are initially equilibrated for a long enough duration. Since the ensemble average attributes of the system are obtained from the long-term average of this data, the succeeding runtime is referred to as the production run. Production run data analysis can yield valuable insights into the simulation system's structural characteristics, including radial distribution functions (RDF) and molecular-level adsorption features (density profile, interaction/bond lengths, and hydrogen bonding)[135].

2.5.2 Ensemble

The adsorption parameters examined in chapters 3 and 4 of this thesis were subjected to MD computations through the NVT and NPT ensembles, respectively. In the NVT Ensemble (canonical ensemble), the number of particles (N), the volume (V), and the temperature (T) are fixed [136]. The system exchanges energy with the surroundings, but the total number of particles and the volume remain constant. According to Andersen (1980), the NPT ensemble requires that the system maintain a constant temperature (T), pressure (P), and the number of molecules (N) [137]. The unit cell vectors remain free to fluctuate, and the volume is changed to alter the pressure. In canonical (NVT) and isothermal-isobaric

(NPT) ensembles, the system is not thermally isolated, and the system's total energy will fluctuate. This feature is implemented via the Nosé-Hoover thermostat in simulations conducted for this thesis [138,139].

2.5.3 Force Field

The force field selection is a crucial step in MD simulations. The force field's functional form is divided into bonded and non-bonded interactions [140,141]. The bonded interaction energies comprise of (a) bond stretching between atoms, (b) bond angle between atoms, and (c) rotation of dihedral angle. Non-bonded energies consist of two primary components: van der Waals interactions, which occur between neutral atoms or molecules and are described by the Lennard–Jones potential, and electrostatic interactions, which involve charged species and are governed by Coulomb's law. In chapters 3 and 4 of this thesis, Dreiding force field describes interatomic interactions during MD simulations. In contrast to many force fields tailored to specific systems, the Dreiding force [134]field aims for broad applicability by using a set of simple and transferable parameters that cover nearly all elements in the periodic table.

2.5.4 Water Models

The interfacial mechanisms of reactant molecule adsorption in an aqueous environment are investigated in the present thesis using molecular dynamics simulations. because water is an essential component of the simulation systems, obtaining accurate MD simulation results requires an accurate water model. Numerous water models are available. Every water model precisely resembled a specific structural characteristic or thermodynamic property of its physical counterpart (condensed phase). The TIP3P [142] water model was utilized in Chapters 3 and 4.

2.5.5 Software Used in Molecular Dynamics Simulations

In this thesis, MD calculations are performed on the supercomputing system (PARAM SHIVAAY supercomputer) at IIT(BHU) using the LAMMPS (Large-scale Atomic/Molecular Massively Parallel System) software [Plimpton (1995)]. While SCIENOMICS's MAPS (Materials and Process Simulation) software, version 4.1.1, was utilized for molecular modeling and analysis[143].

2.5.6 Density functional theory (DFT) calculation

Quantum mechanical calculations involve solving Schrödinger's wave equation using either semi-empirical or ab-initio techniques or Density functional theory (DFT) techniques [144]. Equation 2.7 gives the Schrodinger wave equation.

$$H\Psi = E\Psi \quad \text{……..(2.7)}$$

In eq. 2.7, H represents Hamiltonian operator, E denotes Energy eigenvalue, and Ψ represents wave function. Both ab initio and semi-empirical techniques aim to solve the Schrödinger wave equation for molecular systems in order to determine their energy and wave functions. These parameters efficiently predict a variety of molecular properties. While ab initio methods rely purely on fundamental physical principles without empirical input, and semi-empirical methods introduce system-specific parameters to simplify calculations and to reduce computational cost. Among the ab initio methods, Density functional theory (DFT) stands out as a widely used and powerful tool. Based on quantum mechanics, DFT enables accurate modelling of material properties at the atomistic and electronic levels.

Density-functional theory depend on on the theorem proved by Hohenberg and Kohn, which shows a unique description of a many-body system in terms of the expectation value

of the particle-density operator [145]. The first theorem by Hohenberg and Kohn asserts that *The ground-state energy derived from Schrodinger's equation is a unique functional of the electron density* [145]. In simple words, there exists a one-to-one correspondence between the ground-state wave function and the ground-state electron density. The first theorem offers no insight about the functional. So, the second theorem by Hohenberg and Kohn states: *The true ground-state electron density is the one that minimizes the total energy functional, yielding the full solution to the Schrödinger equation* [146]. Like other *ab initio* methods, DFT is not constrained by parameterization requirements. Consequently, this thesis employs DFT and time-dependent DFT (TD-DFT) to investigate and compute various excited-state electronic structure properties.

TD-DFT offers a formally rigorous extension of the Hohenberg-Kohn-Sham density functional theory (DFT), which is inherently time-independent [147]. TD-DFT addresses systems initially in a stationary ground state and describes their behavior under the influence of a time-dependent perturbation that alters the external potential. The time-dependent self-consistent field (TD-SCF) method was used to calculate the excitation energies. The standard approach to obtaining such time-dependent density involves a modified version of the Kohn-Sham equation, reformulated as the time-dependent Schrödinger equation [147]. Equation 2.8 represents the time-dependent Schrödinger equation.

$$H(t)|\Psi(t)\rangle = i\frac{\partial}{\partial t}|\Psi(t)\rangle \quad \text{.....(2.8)}$$

In eq. 2.8, t is the time, $\Psi(t)\rangle$ denotes the state vector of the quantum system, and H is the Hamiltonian operator. In this thesis, the TD-DFT has been employed to calculate the excited states and model the UV-Visible absorption spectra of molecules. The DFT and TD-DFT calculations allow for the determination of the positions of the frontier orbitals in both the ground and excited states of the molecules.

2.5.7 Basis set and functional

Nobel laureate John Pople was the first to develop the basis sets, which are mathematical functions used to express wave functions and electron densities[148]. The choice of basis set plays a crucial role in determining the efficiency and accuracy of calculations [148]. In chapters 5 and 6, DFT calculations were run using the DGDZVP basis set for all the elements. Chapter 7 used the 6-311G basis set for O and H atoms with DGDZVP pseudopotentials on Ni, Fe, Ag, and I atoms. The DGDZVP basis set is designed to balance computational efficiency and accuracy, incorporating a double-zeta quality (which refers to using two sets of functions to describe each atomic orbital) along with polarization and diffuse functions.

On the other hand, the functionals (in DFT calculations) describe the exchange-correlation energy, which includes the effects of electron-electron interactions in the system. In this thesis, the widely utilized hybrid functional B3LYP was applied for all DFT calculations. B3LYP combines Becke's three-parameter (B3) exchange functional [149]. The functional was used for all geometry optimizations and excited-state calculations.

2.5.8 Software used in the Quantum Mechanical calculations

GaussView 6.0 software is used to draw and analyze the model. The calculations were carried out in the gas phase using the Gaussian 16 program installed on the Centre for Computing and Information Services (CCIS) computer server, IIT BHU.

2.5.9 Plane-wave density functional theory (DFT)

The DFT simulation with plane-wave basis sets is a powerful technique for the study of material properties at the atomistic/electronic level. It can produce various crystal and electronic structure information about semiconductor materials. The entire field of DFT

relies on two fundamental theorems given by Kohn and Hohenberg and some derived equations by Kohn and Sham [150].

Materials are composed of many atoms, which themselves are made up of nuclei surrounded by many-electron wave functions. The nucleus has a significantly larger mass than an electron, causing it to exhibit classical behavior. Therefore, the classical behaviour of nucleus allows the electronic wave function to be decoupled from the nuclear wave function, as described by the Born-Oppenheimer approximation. But, the electron-electron interactions entail solving the many-body Schrodinger equation. The complexity of solving the many-body Schrödinger equation can be reduced using DFT calculations. Because DFT focuses on the electron density rather than the electron wave functions. Equation 2.9 represents the electron density, $n(r)$ at a particular position in space,

$$n(r) = 2 \sum_i \psi_i^*(r)\psi_i(r) \qquad (2.9)$$

In equation 2.9, the symbol $\psi_i(r)$ represents the individual electronic wave function, and the 'asterisk' sign denotes a complex conjugate of the wave function. Here, the summation term shows the probability of finding an electron at position 'r'. Factor 2 represents the two different spins of an electron.

The DFT calculations carried out in the chapter 5 of this thesis used generalized gradient approximations (GGA), and Perdew-Burke-Ernzerhoff (PBE) functional with projector augmented wave (PAW) pseudopotentials. GGA is an extension of the local density approximation (LDA), which can give exchange-correlation energy density. GGA incorporates gradient adjustments to improve the treatment of molecules with nonuniform electron distributions [151].

2.5.10 Software used in the plane wave DFT calculations

All the DFT calculations were performed on Medea molecular modelling software (version 1.0) interface using Vienna Ab-initio Simulation Package (VASP 5.4.4). This software is also installed on the computer server of the Centre for Computing and Information Services (CCIS), IIT BHU.